TECHNICAL ARTICLE

Structural and Raman spectroscopic studies of the two $M_{0.50}SbFe(PO_4)_3$ (M = Mg, Ni) NASICON phases

Abderrahim Aatiq,[a] Asmaa Marchoud, Hajar Bellefqih, and My Rachid Tigha
Département de Chimie, Laboratoire de Physico-Chimie des Matériaux Appliqués, Université Hassan II de Casablanca, Faculté des Sciences Ben M'Sik, Avenue Idriss El harti, B.P. 7955, Casablanca, Morocco

(Received 6 September 2016; accepted 6 March 2017)

Structures of the two $M_{0.50}SbFe(PO_4)_3$ (M = Mg, Ni) phases, abbreviated as [$Mg_{0.50}$] and [$Ni_{0.50}$], were determined at room temperature from X-ray diffraction (XRD) powder data using the Rietveld analysis. Both compounds belong to the NASICON structural family. XRD patterns of [$Mg_{0.50}$] and [$Ni_{0.50}$] phases were easily indexed with a primitive hexagonal unit cell [$P\bar{3}$ space group, $Z = 6$] similar to that already obtained for $La_{0.33}Zr_2(PO_4)_3$. Obtained unit cells parameters are [$a = 8.3443(1)$ Å, $c = 22.3629(1)$ Å], and [$a = 8.3384(1)$, $c = 22.3456(1)$ Å], respectively, for [$Mg_{0.50}$] and [$Ni_{0.50}$] phosphates. In both samples, the $[Sb(Fe)(PO_4)_3]^-$ NASICON framework is preserved and a partially-ordered distribution of Sb^{5+} and Fe^{3+} ions is observed. Raman spectroscopic study was used to obtain further structural information about the nature of bonding in [$Mg_{0.50}$] and [$Ni_{0.50}$] phases.
[doi:10.1017/S0885715617000331]

Key words: iron and antimony phosphate, NASICON structure, Raman spectroscopy, Rietveld analysis

I. INTRODUCTION

The NASICON [acronym for sodium (Na) Super Ionic CONductor] type family has been the subject of intensive research owing to its potential applications as solid electrolyte, electrode material, low thermal expansion ceramics, and as storage materials for nuclear waste (Delmas *et al.*, 1981; Roy *et al.*, 1982; Padhi *et al.*, 1997; Woodcock *et al.*, 1999; Aatiq *et al.*, 2002; Anuar *et al.*, 2014). The structure of such materials with general formula $M_xXX'(PO_4)_3$ consists of a three-dimensional (3D) network made up of corner-sharing $X(X')O_6$ octahedra and PO_4 tetrahedra in such a way that each octahedron is surrounded by six tetrahedra and each tetrahedron is connected to four octahedra. During the past few years, particular attention has been paid to combining titanium or (antimony and iron) and divalent 3*d* transition metals M^{2+}. Most investigations on Nasicon phases with general formula $M_{0.50}Ti_2(PO_4)_3$ (M = Co, Fe, Mg, Mn, Ca) (Barth *et al.*, 1993; El Bouari *et al.*, 1994; Aatiq *et al.*, 2002; Benmokhtar *et al.*, 2007), and $M_{0.50}SbFe(PO_4)_3$ (M = Mn, Cd, Ca, Sr, Pb) (Aatiq *et al.*, 2005, 2006, 2012, 2015) have employed powder X-ray diffraction (XRPD) techniques to probe the global structure of the materials using the Rietveld analysis. For both $M_{0.50}SbFe(PO_4)_3$ and $M_{0.50}Ti_2(PO_4)_3$ NASICON phases series, the structure was already well established when the ionic radii of M^{2+} cations was relatively high and more precisely equal or larger than that of Mn^{2+} ions [i.e., M = Mn, Ca, Cd, Pb, Sr]. Note that all $M_{0.50}SbFe(PO_4)_3$ (M = Mn, Ca, Cd, Pb, Sr) compounds crystallise in the $R\bar{3}$ (No. 148) space group with a practically ordered cationic distribution of M^{2+} cations within the M1 sites. In fact, the same cationic distribution was observed for $M_{0.50}Ti_2(PO_4)_3$ (M = Mn, Ca, Cd, Pb) phases. On the contrary, up to our knowledge, it is noted that an uncertainty exists about the exact symmetry for $M_{0.50}Ti_2(PO_4)_3$ materials containing M^{2+} cations with a relatively small size [e.g., M = Mg, Co]. For example, Barth *et al.* (1993) proposed the $R\bar{3}$ c (No. 167) as the space group for $Mg_{0.50}Ti_2(PO_4)_3$. During their structural discussion, they pointed out a serious problem concerning the two low-intensity reflections observed, in the XRD pattern, respectively at around 12.40° and 12.66° in $2\theta_{Cu}$. Indeed, the origin of these lines does not derive from the method of preparation. Particularly these two lines of XRD diffraction are not generated by the $R\bar{3}c$ space group and also cannot be well attributed to the (101) and/or (003) reflections, which are characteristic of a possible reduction of symmetry from $R\bar{3}c$ to $R\bar{3}$ or $R32$ one. Note that the same problem has been raised by El Bouari *et al.* (1994) for $Co_{0.50}Ti_2(PO_4)_3$ phase who have suggested, in a first time, the refinement in $R\bar{3}c$ space group even if the two low-intensity reflections cited previously are not generated by this space group. In fact, 5 years later and despite the non concordance between the experimental and calculated diffraction lines at around 12.40° and 12.66° in $2\theta_{Cu}$, a reinvestigation of this orthophosphate using optical and magnetic properties leads them to assign in instead the $R32$ or $R\bar{3}$ space groups (Derouet *et al.*, 1999; Olazcuaga *et al.*, 1999). Ten years ago, the reinvestigation of the structure of $La_{0.33}Zr_2(PO_4)_3$ NASICON phases from Neutron and XRDP shows particularly that the reflection around 15° in $2\theta_{Cu}$, which was not generated in the $R\bar{3}c$ space group (Alami *et al.*, 1994) is well indexed in the $P\bar{3}$ (No. 147) space group (Barré *et al.*, 2005, 2006, 2007; Crosnier-Lopez *et al.*, 2006). Thermal study reveals that $La_{0.33}Zr_2(PO_4)_3$ exhibits at high temperature a structural transition from $P\bar{3}$ to $P\bar{3}c$ (No. 165) space groups, which was related to the La^{3+} ion ability to move in the $Zr_2(PO_4)_3$

[a]Author to whom correspondence should be addressed. Electronic mail: a_aatiq@yahoo.fr

framework despite its ionic size (Barré *et al.*, 2006). The $P\bar{3}$-$P\bar{3}c$ phase transition can be explained by the fact that the $P\bar{3}$ space group is a Maximal translationengleiche subgroup of $P\bar{3}c$ one (Hans and Ulrich, 2004). On the other hand, a structural study of $Li_{1-x}La_{x/3}Zr_2(PO_4)_3$ ($0 \leq x \leq 1$) solid solution has shown reversible transition, which is clearly soft and strongly depends of the x value (Barre´ *et al.*, 2007).

Recently, structural characteristics by powder X-ray diffraction (XRD) study using the Rietveld method for $M_{0.50}SbFe(PO_4)_3$ (M = Mn, Cd, Ca, Sr, Pb) showed that all samples crystallise in the $R\bar{3}$ space group and the M^{2+} ions occupied practically one-half of the M1 sites. The Sb^{5+} and Fe^{3+} cations are also orderly distributed within the SbFe $(PO_4)_3$ NASICON framework (Aatiq *et al.*, 2005, 2006, 2012, 2015). Note that because of the fast diffusion of Na^+ ions in the NASICON framework, the $M_{0.5}SbFe(PO_4)_3$ phases can be tested as Negative Electrode materials in Na-Ion and Li-Ion Batteries as was more recently reported as example for the $Mg_{0.5}Ti_2(PO_4)_3$ NASICON phase (Zhao *et al.*, 2017).

In a continuation of our search concerning NASICON-like phases herein we report the results of the structural investigation by the Rietveld refinement using the XRD patterns of the two $M_{0.50}SbFe(PO_4)_3$ (M = Mg, Ni) phases, abbreviated as [$Mg_{0.50}$] and [$Ni_{0.50}$]. During this work we examined some additional reflections, which appeared in the experimental XRD patterns. It should be noticed that the observed small additional reflections within the XRD spectra cannot be indexed successfully with either $R\bar{3}c$ or $R\bar{3}$ space groups. In order to obtain further structural information about the nature of bonding in the two [$Mg_{0.50}$] and [$Ni_{0.50}$] phosphates, a Raman spectroscopic study involving the factor group analysis was also undertaken.

II. EXPERIMENTAL

Syntheses of $M_{0.50}SbFe(PO_4)_3$ (M = Mg, Ni) phases were carried out using conventional solid-state reaction techniques. Powder crystalline samples were prepared from mixtures of oxides MO (M = Mg, Ni) (Riedel-de Haën, 99%), Sb_2O_3 (Riedel-de Haën, 99.9 %), Fe_2O_3 (Prolabo, 99%), and $NH_4H_2PO_4$ (Riedel-de Haën, 99%) in stoichiometric proportions. The mixture was heated progressively with intermittent grinding at 200 °C (12 h), 400 °C (6 h), 600 °C (12 h), 800 °C (24 h), 900 °C (24 h), and 950 °C (24 h) in air atmosphere.

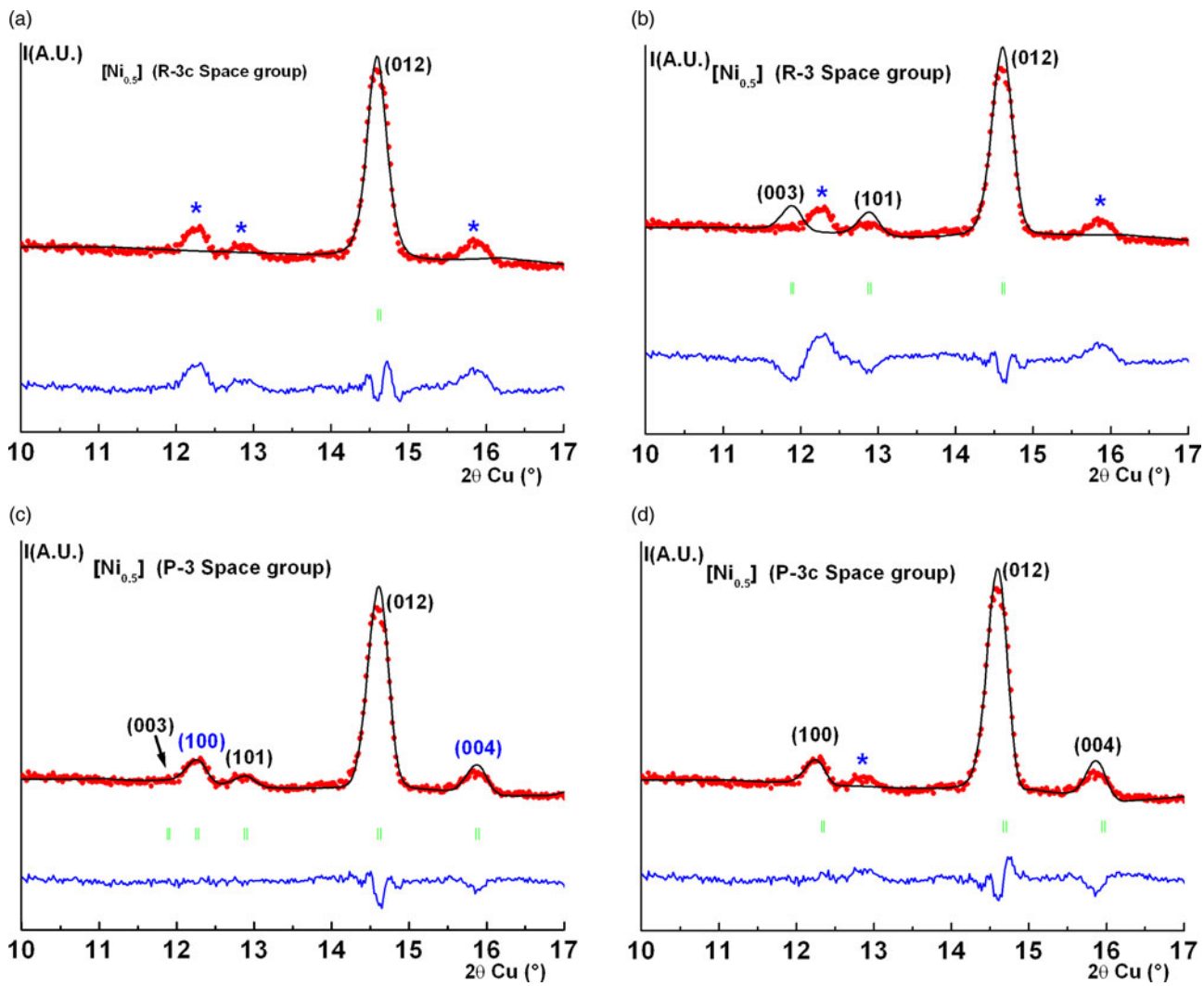

Figure 1. (Color online) Comparison of the experimental (•••) calculated (—), and difference profile of the XRD pattern of $Ni_{0.50}SbFe(PO_4)_3$. The *LeBail* refinements of cell parameters were made for (a) $R\bar{3}c$, (b) $R\bar{3}$, (c) $P\bar{3}$, and (d) $P\bar{3}c$ space groups over the range 10°–17° (2θ Cu). The non-indexed XRD diffraction lines are indicated by blue stars.

https://doi.org/10.1017/S0885715617000331 Published online by Cambridge University Press

The products of reaction were characterised by XRD at room temperature with a Panalytical X′Pert-PRO (θ–2θ) diffractometer equipped with x'celerator detector; (Cu$K\alpha$) radiation (45 kV, 40 mA); divergence slit of 1°, receiving slit of 0.10 mm, and antiscatter slit of 1°. The data were collected from 10° to 90°2θ, in steps of 0.02°, with a counting time of 15 s per step. The Rietveld refinement of the structure was performed using the Fullprof program (Rodriguez-Carvajal, 1997).

The Raman spectra are recorded on RENISHAW 1000B spectrometer in the wave number range 100–1500 cm^{-1}. All the spectra have been recorded at room temperature.

III. RESULTS AND DISCUSSION

A. Structure of $M_{0.50}$SbFe(PO$_4$)$_3$ (M = Mg, Ni) phases

Analysis of the XRPD spectra for the two $M_{0.50}$SbFe(PO$_4$)$_3$ (M = Mg, Ni) materials indicated that the principal peak positions of the XRD lines are similar to those observed for other NASICON-type phases. At first sight, it seems that the existing low-intensity lines in the XRD pattern of [Mg$_{0.50}$] and [Ni$_{0.50}$] phases can be indexed in the usual $R\bar{3}c$ or $R\bar{3}$ space groups but a *LeBail* fit (profile matching) program (LeBail *et al.*, 1988), realised for both materials and in the two possible space groups, shows clearly that some additional reflections with a relatively low intensity are not indexed. A comparison between experimental, calculated and difference profile of the XRD pattern for [Ni$_{0.50}$] phase, in the selected 10°–17° angular range in $2\theta_{Cu}$, are given as example in Figure 1. In fact, the initial findings show clearly that in the $R\bar{3}c$ space group several lines of XRD diffraction, which are indicated by blue stars, are not indexed [Figure 1(a)]. Note also that the two usually known (101) and (003) reflections, which are characteristic of the $R\bar{3}$ space group are not a good fit to the experimental pattern [Figure 1(b)]. In regards to our tested *LeBail* fit refinement in both $R\bar{3}c$ and $R\bar{3}$ space group, obtained results are comparable with those already signalised for $M_{0.50}$Ti$_2$(PO$_4$)$_3$ (M = Mg, Co) NASICON phases (Barth *et al.*, 1993; El Bouari *et al.*, 1994). Consequently, it is clear that the two rhombohedral $R\bar{3}c$ or $R\bar{3}$ space groups usually encountered for many NASICON–type phases are excluded here. On the other hand, given that the $P\bar{3}$ (No. 147) space group is a Maximal klassengleiche subgroup of $R\bar{3}$ (No. 148) as a result of the loss of centring translations (Hans and Ulrich, 2004), and according to the structural study recently realised for similar phosphates with NASICON like phases such as La$_{0.33}$Zr$_2$(PO$_4$)$_3$ (Barré *et al.*, 2005), the model of the *LeBail* refinement in the $P\bar{3}$ space group is tested. In this case, a good concordance between the experimental and calculated profile of the XRD pattern is obtained [Figure 1(c)]. In fact, the non-indexed diffraction lines in the two rhombohedral space groups $R\bar{3}c$ or $R\bar{3}$ are generated by the $P\bar{3}$ space group. In the case of $Ln_{0.33}$Zr$_2$(PO$_4$)$_3$ (Ln = Ce, Eu, Yb) phases, the already obtained results from the Rietveld refinement study, using the powder XRD data, have shown that they were indexed in the $P\bar{3}c$ space group (Bykov *et al.*, 2006). It should be noticed that the $P\bar{3}$ space group is also a Maximal translationengleiche subgroup of $P\bar{3}c$ one. Hence, a comparison between experimental, calculated and difference profile of the XRD pattern for the selected [Mg$_{0.50}$] phase, in both $P\bar{3}$ and $P\bar{3}c$ space group, are realised and given as example in the selected 18°–42° ($2\theta_{Cu}$) angular range (Figure 2). For more details, the experimental, calculated and difference profile of the XRD pattern for [Ni$_{0.50}$], in the selected 10°–17° ($2\theta_{Cu}$) angular range, are also given for comparison in Figure 1(d). In fact, because of the loss of

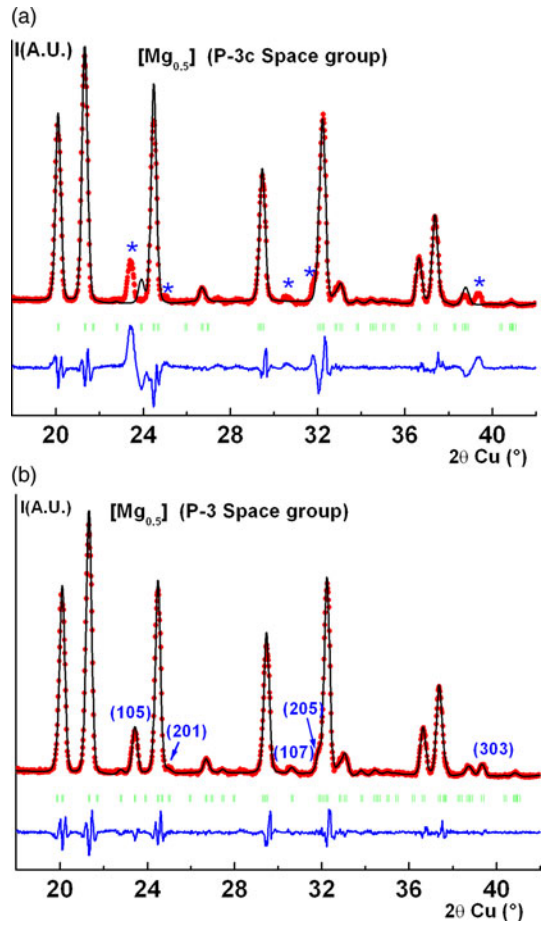

Figure 2. (Color online) Comparison of the experimental (•••) calculated (—), and difference profile of the XRD pattern of Mg$_{0.50}$SbFe(PO$_4$)$_3$. The *LeBail* refinements of cell parameters were made for (a) $P\bar{3}c$, and (b) $P\bar{3}$ space groups over the range 18°–42° (2θ Cu). The non-indexed XRD diffraction lines are indicated by blue stars.

TABLE I. $R\bar{3}$-$P\bar{3}$ transposition of the atomic positions from $M_{0.50}X'_2$(PO$_4$)$_3$ ($R\bar{3}$ space group) to $M_{0.50}X_2$(PO$_4$)$_3$ ($P\bar{3}$ space group) NASICON phases.

$R\bar{3}$ (No. 148)	$P\bar{3}$ (No. 147)
$M1$(3a) 3a (0, 0, 0)	M(1a) 1a, (0, 0, 0)
	M(2d) 2d, (1/3, 2/3, z): z = 2/3
$M1$(3b) 3b (0, 0, 1/2)	M(1b) 1b, (0, 0, 1/2)
	M(2d′) 2d', (1/3, 2/3, z): z = 2/3 + 1/2
X'(1) 6c, (0, 0, ~0.14)	X(1) 2c, (0, 0, ~0.14)
	X(3) 2d, (2/3, 1/3, ~0.17)
	X(4) 2d, (2/3, 1/3, ~0.49)
X'(2) 6c, (0, 0, ~0.64)	X(2) 2c, (0, 0, ~0.64)
	X(5) 2d, (2/3, 1/3, ~0.69)
	X(6) 2d, (2/3, 1/3, ~0.97)
P 18f, (x, y, z) (0.28, 0.01, 0.25)	P(1) 6 g, (x, y, z) (~0.28, ~0.01, ~0.25)
	P(2) 6 g, (x, y, z) (~0.95, ~0.31, ~0.55)
	P(3) 6 g, (x, y, z) (~0.61, ~0.65, ~0.91)
O 4 × 18f, (x, y, z)	O 12 × 6 g, (x, y, z)

https://doi.org/10.1017/S0885715617000331 Published online by Cambridge University Press

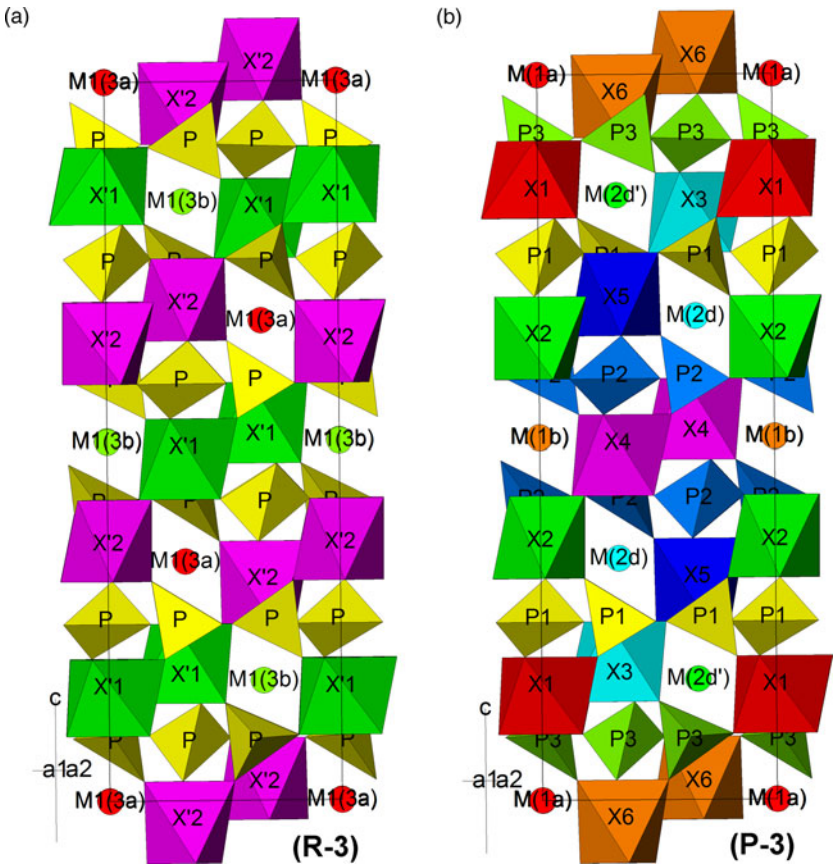

Figure 3. (Color online) Projections of the structure for (a) $M_{0.50}X'_2(PO_4)_3$ ($R\bar{3}$ space group), and (b) $M_{0.50}X_2(PO_4)_3$ ($P\bar{3}$ space group) along the *b*-axis. The different *M* and *X* sites, accompanying the $R\bar{3}$-$P\bar{3}$ transposition of atomic positions, have been labelled and located.

TABLE II. Results of the Rietveld refinement of $Mg_{0.50}SbFe(PO_4)_3$.

$Mg_{0.50}[SbFe]_X(PO_4)_3 = Mg_{0.50}X_2(PO_4)_3$

Space group: $P\bar{3}$; [$Z = 6$, $a = 8.3443(1)$ Å, $c = 22.3629(1)$ Å; $V = 1348(1)$ Å^3]
Experimental data
Temperature, 298 K ; angular range, $10° \leq 2\theta \leq 90°$; step scan increment ($2\theta$), 0.02°
Zero point (2θ), −0.039(2)°
Profile parameters
Pseudo-Voigt function, PV = ηL + (1 - η)G; $\eta = 0.271(2)$
Half-width parameters, $U = 0.166(2)$, $V = -0.101(2)$, and $W = 0.091(1)$
Conventional Rietveld R-factors, $R_{WP} = 9.5$; $R_P = 7.7$; $R_B = 6.3$; $R_F = 5.0\%$

Atom	Site	Wyckoff positions			B_{iso}(Å^2)	Occupancy
Mg(1b)	1*b*	0	0	0.5	2.20(2)	1
Mg(2d′)	2*d*	1/3	2/3	0.1667(1)	2.20(2)	1
X(1) = Sb/Fe(1)	2*c*	0	0	0.1585(5)	0.62(1)	1.20/0.80
X(2) = Sb/Fe(2)	2*c*	0	0	0.6413(6)	0.62(1)	0.80/1.20
X(3) = Sb/Fe(3)	2*d*	2/3	1/3	0.1748(5)	0.62(1)	1.20/0.80
X(4) = Sb/Fe(4)	2*d*	2/3	1/3	0.4918(5)	0.62(1)	1.20/0.80
X(5) = Sb/Fe(5)	2*d*	2/3	1/3	0.6920(6)	0.62(1)	0.80/1.20
X(6) = Sb/Fe(6)	2*d*	2/3	1/3	0.9747(5)	0.62(1)	0.80/1.20
P(1)	6*g*	0.2965(3)	−0.0112(5)	0.2511(4)	2.05(2)	1
P(2)	6*g*	0.9632(4)	0.3221(3)	0.5844(4)	2.05(2)	1
P(3)	6*g*	0.6298(3)	0.6554(4)	0.9178(4)	2.05(2)	1
O(1)	6*g*	0.167(1)	0.927(1)	0.197(1)	2.10(3)	1
O(2)	6*g*	0.834(1)	0.272(1)	0.531(1)	2.10(3)	1
O(3)	6*g*	0.500(1)	0.605(1)	0.864(1)	2.10(3)	1
O(4)	6*g*	0.204(1)	0.018(1)	0.306(1)	2.10(3)	1
O(5)	6*g*	0.537(1)	0.685(1)	0.973(1)	2.10(3)	1
O(6)	6*g*	0.871(1)	0.351(1)	0.639(1)	2.10(3)	1
O(7)	6*g*	0.185(1)	0.172(1)	0.091(1)	2.10(3)	1
O(8)	6*g*	0.135(1)	0.515(1)	0.580(1)	2.10(3)	1
O(9)	6*g*	0.469(1)	0.1815	0.246(1)	2.10(3)	1
O(10)	6*g*	0.870(1)	0.811(1)	0.580(1)	2.10(3)	1
O(11)	6*g*	0.635(1)	0.478(1)	0.913(1)	2.10(3)	1
O(12)	6*g*	0.294(1)	−0.194(1)	0.246(1)	2.10(3)	1

https://doi.org/10.1017/S0885715617000331 Published online by Cambridge University Press

TABLE III. Results of the Rietveld refinement of $Ni_{0.50}SbFe(PO_4)_3$.

$Ni_{0.50}[SbFe]_X(PO_4)_3 = Ni_{0.50}X_2(PO_4)_3$						
Space group: $P\bar{3}$; [$Z = 6$, $a = 8.3384(1)$ Å, $c = 22.3456(1)$ Å; $V = 1345(1)$ Å^3]						
Experimental data						
Temperature, 298 K; angular range, $10° \leq 2\theta \leq 90°$; step scan increment ($2\theta$), 0.02°						
Zero point (2θ), −0.003(1)°						
Profile parameters						
Pseudo-Voigt function, PV = ηL + (1 - η)G; $\eta = 0.146(2)$						
Half-width parameters, $U = 0.343(2)$, $V = -0.143(2)$, and $W = 0.105(1)$						
Conventional Rietveld R-factors, $R_{WP} = 9.7$; $R_P = 7.8$; $R_B = 6.6$; $R_F = 4.2\%$						
Atom	Site	Wyckoff positions			B_{iso}(Å^2)	Occupancy
Ni(1b)	1*b*	0	0	0.5	2.5(1)	1
Ni(2d′)	2*d*	1/3	2/3	0.1667(1)	2.5(1)	1
$X(1)$ = Sb/Fe(1)	2*c*	0	0	0.1567(4)	0.8(1)	1.50/0.50
$X(2)$ = Sb/Fe(2)	2*c*	0	0	0.6415(5)	0.8(1)	0.50/1.50
$X(3)$ = Sb/Fe(3)	2*d*	2/3	1/3	0.1766(4)	0.8(1)	1.50/0.50
$X(4)$ = Sb/Fe(4)	2*d*	2/3	1/3	0.4900(5)	0.8(1)	1.50/0.50
$X(5)$ = Sb/Fe(5)	2*d*	2/3	1/3	0.6918(4)	0.8(1)	0.50/1.50
$X(6)$ = Sb/Fe(6)	2*d*	2/3	1/3	0.9749(5)	0.8(1)	0.50/1.50
P(1)	6*g*	0.2848(4)	−0.0151(5)	0.2465(4)	2.1(1)	1
P(2)	6*g*	0.9514(5)	0.3182(4)	0.5798(5)	2.1(1)	1
P(3)	6*g*	0.6181(5)	0.6515(4)	0.9132(5)	2.1(1)	1
O(1)	6*g*	0.148(1)	0.927(1)	0.196(1)	2.5(1)	1
O(2)	6*g*	0.833(1)	0.255(1)	0.523(1)	2.5(1)	1
O(3)	6*g*	0.499(1)	0.589(1)	0.856(1)	2.5(1)	1
O(4)	6*g*	0.192(1)	0.033(1)	0.297(1)	2.5(1)	1
O(5)	6*g*	0.539(1)	0.704(1)	0.968(1)	2.5(1)	1
O(6)	6*g*	0.860(1)	0.359(1)	0.632(1)	2.5(1)	1
O(7)	6*g*	0.190(1)	0.170(1)	0.090(1)	2.5(1)	1
O(8)	6*g*	0.155(1)	0.446(1)	0.562(1)	2.5(1)	1
O(9)	6*g*	0.489(1)	0.112(1)	0.229(1)	2.5(1)	1
O(10)	6*g*	0.870(1)	0.810(1)	0.580(1)	2.5(1)	1
O(11)	6*g*	0.627(1)	0.472(1)	0.913(1)	2.5(1)	1
O(12)	6*g*	0.294(1)	−0.195(1)	0.246(1)	2.5(1)	1

c-plane in transforming from space group $P\bar{3}c$ to the space group $P\bar{3}$, some diffraction lines of the experimental XRD patterns indicated in the Figure 2 by blue stars are indexed only in the $P\bar{3}$ space group. It should be noticed that all obtained results, from *LeBail* fit, agree well with the choice of $P\bar{3}$ space group for both [$Mg_{0.50}$] and [$Ni_{0.50}$] materials.

Given that there is an important number of parameter to be refined during different steps of the Rietveld refinement in the $P\bar{3}$ space group, a strategy of structural refinement was followed. Note that in $La_{0.33}Zr_2(PO_4)_3$ there is only one type of atom (i.e., one Zr atom) per *X* site, therefore the determination of the amount of existing cation in each *X* site within the [$X_2(PO_4)_3$] framework was not raised. Indeed, in our case, this problem should be resolved before starting the Rietveld refinement in the $P\bar{3}$ space group. In a first time, the Rietveld refinement was carried out in $R\bar{3}$ space group and

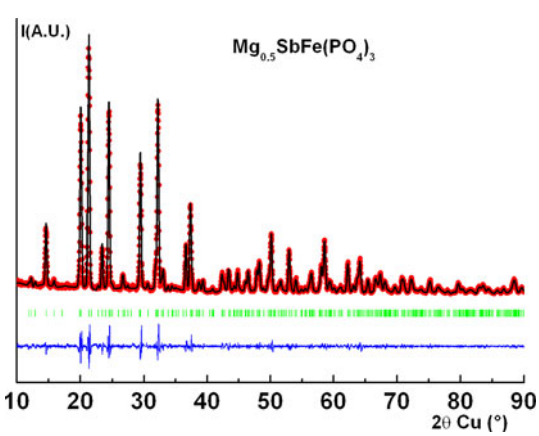

Figure 4. (Color online) Experimental (•••) calculated (—), and difference profile, obtained after Rietveld refinement, of the XRD pattern of $Mg_{0.50}SbFe(PO_4)_3$.

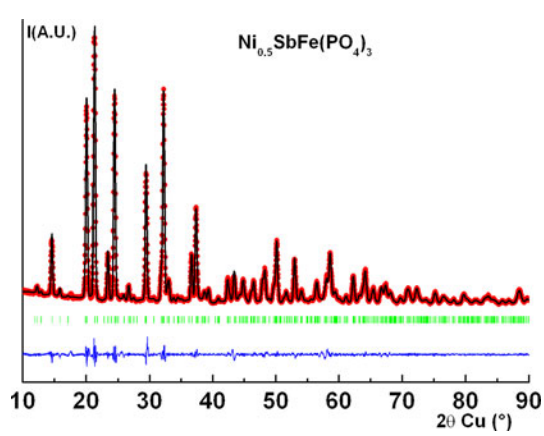

Figure 5. (Color online) Experimental (•••) calculated (—), and difference profile, obtained after Rietveld refinement, of the XRD pattern of $Ni_{0.50}SbFe(PO_4)_3$.

https://doi.org/10.1017/S0885715617000331 Published online by Cambridge University Press

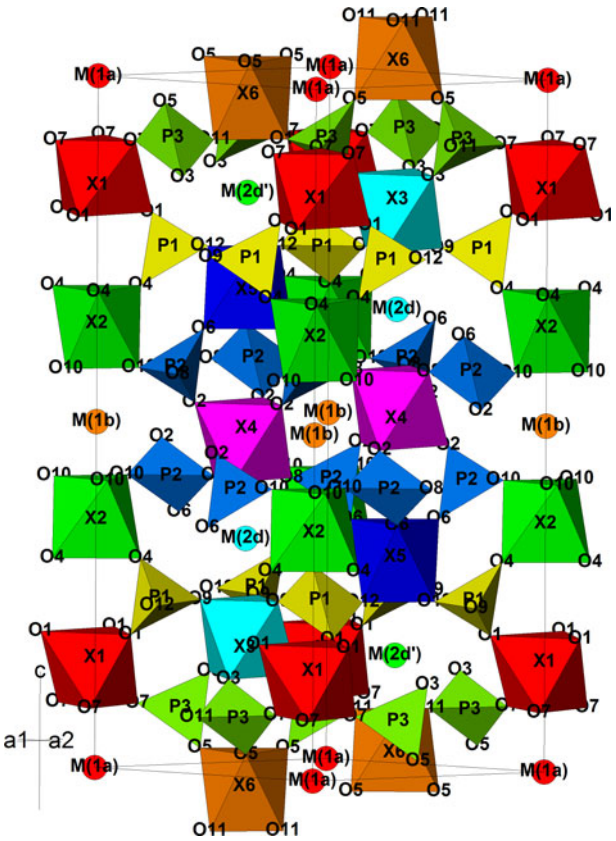

Figure 6. (Color online) View of the structure for $M_{0.50}X_2(PO_4)_3$ [M = Mg, Ni; X = Sb(Fe)] NASICON-type phases.

the structural parameters of $Mn_{0.50}SbFe(PO_4)_3$ (Aatiq *et al.*, 2005) were chosen as starting model. In fact, despite the none perfect concordance for some reflections of low intensity in the XRD spectra for both [$Mg_{0.50}$] and [$Ni_{0.50}$] materials, the obtained results of refinements in $R\bar{3}$ space group will give particularly interesting data about the future Sb^{5+} and Fe^{3+} cationic distribution within the [$SbFe(PO_4)_3$] NASICON frameworks when the refinement is realised in the $P\bar{3}$ space group. Results of refinement, in $R\bar{3}$ space group, show that Ni^{2+} in [$Ni_{0.50}$] and Mg^{2+} in [$Mg_{0.50}$] are distributed over $M1$ sites in an ordered manner along the c-axis. They are located in $3b$ sites (0 0 1/2) with a complete occupancy, $3a$ sites (0 0 0) remain vacant. For [$Mg_{0.50}$], the obtained occupancy rate of Sb^{5+} and Fe^{3+} cations, within the two possible $6c$ sites are, respectively, 1.20(1)/0.80(1) for Sb^{5+}/Fe^{3+} in $X'(1)$ (0 0–0.14) position, and 0.80(1)/1.20 (1) for the Sb^{5+}/Fe^{3+} in $X'(2)$ (0 0–0.64) one. In the case of [$Ni_{0.50}$] phase, obtained cationic distribution are 1.50(1)/0.50 (1) for Sb^{5+}/Fe^{3+} in the $X'(1)$ position and 0.50(1)/1.50(1) for Sb^{5+}/Fe^{3+} in the $X'(2)$ one. Note that during the Rietveld refinement in $P\bar{3}$ space group, it is not easy to determine without ambiguity the occupancy rate of Sb^{5+} and Fe^{3+} cations within every X site position among the six existing one [i.e., $X(1)$, $X(2)$, $X(3)$, $X(4)$, $X(5)$, $X(6)$]. So, realistic occupancy rates of Sb(Fe) cations within the framework can be deduced from the values obtained during the refinement in $R\bar{3}$ space group. In the following, obtained structural parameters of our Rietveld refinement, in $R\bar{3}$ space group, were used as starting structural parameters for refinements in the $P\bar{3}$ space group but after a transposition from $R\bar{3}$ to $P\bar{3}$ space groups. The corresponding splitting of possible atomic positions was given in Table I. As was shown in the Figure 3 and according to the data mentioned in Table I, this last point was also clarified by comparing projections of structures of the two NASICON-type phases, $M_{0.50}X'_2(PO_4)_3$ refined in the $R\bar{3}$ space group [Figure 3(a)] and the $M_{0.50}X_2(PO_4)_3$, which will be refined later in the $P\bar{3}$ one [Figure 3(b)]. On the other hand, by examining the large number of structural parameters that need to be refined in the $P\bar{3}$ space group for [$Mg_{0.50}$] and [$Ni_{0.50}$], a realistic convergence of the refinement is reached by using soft-constrained P–O and Sb(Fe)–O distances [i.e., 1.52 (1) and 2.00(1) Å for P–O and Sb(Fe)–O, respectively]. By performing the $R\bar{3}$-$P\bar{3}$ transposition of atomic positions outlined in Table I, we can conclude that the three M^{2+} cations of the unit cell are preferentially located as follows: one in the M(1b) (0, 0, 0.5) site and the two other ones are in the M(2d′) (1/3, 2/3, ∼0.17) site. Both M(1b) and M(2d′) sites correspond to the $M1$(3b) sites frequently reported in NASICON structure with $R\bar{3}$ space group (Table I and Figure 3). As it will

TABLE IV. Selected interatomic distances (Å) and calculated bond valence sum (BVS) for $Mg_{0.50}SbFe(PO_4)_3$.

$Mg_{0.50}[SbFe]_X(PO_4)_3 = Mg_{0.50}X_2(PO_4)_3$		
X–O distances (Å)	X–O distances (Å)	X–O distances (Å)
$3 \times X(1)$-O(1) = 1.980(5)	$3 \times X(3)$–O(3) = 1.918(5)	$3 \times X(5)$–O(6) = 2.012(5)
$3 \times X(1)$-O(7) = 2.122(5)	$3 \times X(3)$–O(9) = 2.185(5)	$3 \times X(5)$–O(12) = 1.941(5)
⟨Aver. $X(1)$-O⟩ = 2.05(1)	Aver. ⟨$X(3)$–O⟩ = 2.05(1)	Aver. ⟨$X(5)$-O⟩ = 1.98(1)
BVS [$X(1)$] = 3.8	BVS [$X(3)$] = 3.8	BVS [$X(5)$] = 4.5
(should be 3.8)	(should be 3.8)	(should be 3.8)
$3 \times X(2)$–O(4) = 2.012(5)	$3 \times X(4)$–O(2) = 1.918(5)	$3 \times X(6)$–O(5) = 2.012(5)
$3 \times X(2)$–O(10) = 1.959(5)	$3 \times X(4)$–O(8) = 2.201(5)	$3 \times X(6)$–O(11) = 1.940(5)
Aver. ⟨$X(2)$–O⟩ = 1.98(1)	Aver. ⟨$X(4)$–O⟩ = 2.06(1)	Aver. ⟨$X(6)$–O⟩ = 1.98(1)
BVS [$X(2)$] = 4.5	BVS [$X(4)$] = 3.8	BVS [$X(6)$] = 4.5
(should be 3.8)	(should be 3.8)	(should be 3.8)
P(1)–O distances (Å)	P(2)–O distances (Å)	P(3)–O distances (Å)
P(1)–O(1) = 1.519(4)	P(2)–O(2) = 1.524(4)	P(3)–O(3) = 1.524(4)
P(1)–O(4) = 1.534(4)	P(2)–O(6) = 1.535(4)	P(3)–O(5) = 1.534(4)
P(1)–O(9) = 1.533(4)	P(2)–O(8) = 1.532(4)	P(3)–O(7) = 1.508(4)
P(1)–O(12) = 1.519(4)	P(2)–O(10) = 1.521(4)	P(3)–O(11) = 1.503(4)
Aver. ⟨P(1)-O⟩ = 1.53(1)	Aver. ⟨<P(2)-O⟩ = 1.53(1)	Aver. ⟨ P(3)–O⟩ = 1.52(1)
BVS [P(1)] = 4.9	BVS [P(2)] = 4.6	BVS [P(3)] = 4.6
(should be 5)	(should be 5)	(should be 5)

https://doi.org/10.1017/S0885715617000331 Published online by Cambridge University Press

TABLE V. Selected interatomic distances (Å) and calculated bond valence sum (BVS) for $Ni_{0.50}SbFe(PO_4)_3$.

$Ni_{0.50}[SbFe]_X(PO_4)_3 = Ni_{0.50}X_2(PO_4)_3$		
X–O distances (Å)	*X*–O distances (Å)	*X*–O distances (Å)
3 × *X*(1)–O(1) = 1.904(5)	3 × *X*(3)–O(3) = 1.941(5)	3 × *X*(5)–O(6) = 2.021(5)
3 × *X*(1) –O(7) = 2.043(5)	3 × *X*(3)–O(9) = 2.056(5)	3 × *X*(5)–O(12) = 1.937(5)
⟨Aver. *X*(1) –O⟩ = 1.97(1)	Aver. ⟨*X*(3)-O⟩ = 2.00(1)	Aver. ⟨*X*(5)-O⟩ = 1.98(1)
BVS [*X*(1)] = 4.5	BVS [*X*(3)] = 4.6	BVS [*X*(5)] = 4.0
(should be 4.5)	(should be 4.5)	(should be 3.5)
3 × *X*(2)-O(4) = 2.024(5)	3 × *X*(4)–O(2) = 1.943(5)	3 × *X*(6)–O(5) = 2.033(5)
3 × *X*(2)-O(10) = 1.964(5)	3 × *X*(4)–O(8) = 2.057(5)	3 × *X*(6)–O(11) = 1.932(5)
Aver. ⟨*X*(2)-O⟩ = 1.99(1)	Aver. ⟨*X*(4)-O⟩ = 2.00(1)	Aver. ⟨*X*(6)-O⟩ = 1.98(1)
BVS [*X*(2)] = 4.0	BVS [*X*(4)] = 4.6	BVS [*X*(6)] = 4.0
(should be 3.5)	(should be 4.5)	(should be 3.5)
P(1)–O distances (Å)	P(2)–O distances (Å)	P(3)–O distances (Å)
P(1)–O(1) = 1.502(4)	P(2)–O(2) = 1.534(4)	P(3)–O(3) = 1.538(4)
P(1)–O(4) = 1.529(4)	P(2)–O(6) = 1.524(4)	P(3)–O(5) = 1.554(4)
P(1)–O(9) = 1.539(4)	P(2)–O(8) = 1.538(4)	P(3)–O(7) = 1.549(4)
P(1)–O(12) = 1.538(4)	P(2)–O(10) = 1.524(4)	P(3)–O(11) = 1.537(4)
Aver. ⟨P(1)–O⟩ = 1.53(1)	Aver. ⟨P(2)-O⟩ = 1.53(1)	Aver. ⟨P(3)-O⟩ = 1.54(1)
BVS [P(1)] = 4.9	BVS [P(2)] = 4.6	BVS [P(3)] = 4.6
(should be 5)	(should be 5)	(should be 5)

be shown later, this cationic distribution is in good agreement with the obtained M^{2+}-O (M = Mg, Ni) distance values. The final reliability factors and atomic parameters for [$Mg_{0.50}$] and [$Ni_{0.50}$] phases are summarised in Tables II and III, respectively. A comparison of the experimental and calculated XRD profiles, after Rietveld refinement, of [$Mg_{0.50}$] and [$Ni_{0.50}$] is shown in Figures 4 and 5, respectively. A view of the structure of $M_{0.50}Sb(Fe)(PO_4)_3$ (M = Mg, Ni) NASICON

TABLE VI. Powder diffraction data of $Mg_{0.50}SbFe(PO_4)_3$ (Cu$K\alpha_1$; λ = 1.540 56 Å).

hkl	d_{obs} (Å)	$2\theta_{obs}$ (°)	$(2\theta_{obs}-2\theta_{calc})$ (°)	I/I_0 (obs)	I/I_0 (calc)	*hkl*	d_{obs} (Å)	$2\theta_{obs}$ (°)	$(2\theta_{obs}-2\theta_{calc})$ (°)	I/I_0 (obs)	I/I_0 (calc)
100	7.2252	12.24	−0.006	40	40	314	1.8864	48.202	0.02	110	110
101	6.8752	12.866	−0.005	20	20	129	1.8378	49.561	−0.025	35	35
102	6.0684	14.585	0.009	250	260	226	1.8201	50.076	0.014	220	220
004	5.5903	15.84	−0.011	37	37	402	1.7832	51.186	−0.023	16	16
005	4.4723	19.836	0.013	167	167	0 2 11	1.7716	51.545	0.013	32	32
104	4.4214	20.067	0.008	688	720	21 10	1.7301	52.876	0.01	150	150
110	4.1715	21.282	−0.011	999	999	317	1.6975	53.972	0.005	35	35
105	3.8027	23.374	0.012	170	175	1 0 13	1.6733	54.818	0.021	10	10
113	3.6402	24.433	−0.002	710	740	2 0 12	1.6561	55.437	0.023	10	10
200	3.6126	24.623	−0.007	270	270	3 0 10	1.6387	56.077	0.02	35	30
201	3.5664	24.947	0.013	30	30	1 2 11	1.6306	56.379	0.018	56	50
114	3.3433	26.641	0.006	62	62	1 1 13	1.5902	57.946	0.01	94	90
115	3.0505	29.253	−0.007	212	212	140	1.5767	58.492	0.008	190	180
024	3.0342	29.414	−0.008	492	536	0 1 14	1.5596	59.196	0.03	35	35
107	2.9216	30.574	0.013	20	20	413	1.5425	59.917	0.012	10	10
205	2.8103	31.817	0.018	100	100	326	1.5145	61.142	0.01	10	10
008	2.7951	31.993	0.007	215	215	3 1 10	1.4923	62.151	0.012	110	100
116	2.7792	32.182	0.008	730	730	2 3 7	1.4713	63.141	0.012	10	10
210	2.7309	32.768	−0.012	50	50	049	1.461	63.638	0.01	35	35
211	2.7107	33.018	−0.009	76	76	146	1.4521	64.076	0.005	120	110
122	2.6529	33.759	0.015	15	15	1 3 11	1.4271	65.335	0.01	35	35
018	2.6069	34.373	0.013	10	10	1 1 15	1.4038	66.559	0.03	35	35
214	2.4537	36.592	0.011	180	180	330	1.3905	67.28	0.01	70	60
300	2.4084	37.306	0.01	330	330	0 2 15	1.378	67.971	0.02	30	30
301	2.3945	37.53	−0.009	80	80	0 4 11	1.3503	69.567	0.015	10	10
215	2.3307	38.598	0.004	34	34	2 3 10	1.3316	70.685	0.013	35	35
118	2.3221	38.748	0.013	30	30	2 2 13	1.327	70.966	0.02	30	30
303	2.2917	39.281	−0.016	30	30	2 1 15	1.3085	72.129	0.03	40	40
119	2.1346	42.306	0.012	56	56	2 2 14	1.2681	74.809	0.01	30	30
305	2.1205	42.602	0.02	26	26	600	1.2042	79.535	0.001	20	20
220	2.0857	43.347	−0.012	70	75	4 2 10	1.1653	82.752	0.01	30	20
209	2.0472	44.206	0.022	16	16	520	1.1569	83.487	0.011	40	40
306	2.0228	44.768	0.012	70	70	5 1 10	1.1224	86.677	0.012	30	30
312	1.9725	45.974	−0.014	30	30	01 20	1.1049	88.399	0.01	20	20
224	1.9542	46.43	0.011	60	60	1 5 11	1.0938	89.534	0.009	10	10
128	1.9533	46.45	−0.01	64	64						
20 10	1.9014	47.799	0.015	70	70						

https://doi.org/10.1017/S0885715617000331 Published online by Cambridge University Press

TABLE VII. Powder diffraction data of $Ni_{0.50}SbFe(PO_4)_3$ (Cu$K\alpha_1$; λ = 1.540 56 Å).

hkl	d_{obs} (Å)	$2\theta_{obs}$ (°)	$(2\theta_{obs} - 2\theta_{calc})$ (°)	I/I_0 (obs)	I/I_0 (calc)	*hkl*	d_{obs} (Å)	$2\theta_{obs}$ (°)	$(2\theta_{obs} - 2\theta_{calc})$ (°)	I/I_0 (obs)	I/I_0 (calc)
100	7.2213	12.246	−0.001	30	20	129	1.8366	49.607	−0.015	40	30
101	6.8714	12.873	−0.001	20	20	226	1.819	50.11	0.004	260	260
102	6.0648	14.595	0.001	240	250	402	1.7822	51.213	−0.003	10	10
004	5.5864	15.859	0.008	20	20	0 2 11	1.7704	51.601	0.003	40	40
005	4.4691	19.86	0.01	150	150	21 10	1.729	52.927	0.016	170	180
104	4.4185	20.085	0.006	700	710	317	1.6966	54.01	0.005	40	30
110	4.1692	21.292	−0.002	999	999	1 0 13	1.6721	54.886	0.02	10	10
112	3.9061	22.747	−0.01	10	10	2 0 12	1.655	55.499	0.02	10	10
105	3.8002	23.397	0.001	160	170	0 3 10	1.6377	56.129	0.02	20	30
113	3.6381	24.449	−0.002	700	730	1 2 11	1.6296	56.435	0.018	50	40
200	3.6106	24.634	−0.002	330	330	1 1 13	1.5891	58.015	0.01	90	90
201	3.5644	24.959	0.015	20	20	140	1.5758	58.522	0.003	150	140
114	3.3413	26.661	0.001	50	50	0 1 14	1.5585	59.271	0.03	40	40
115	3.0486	29.277	0.005	170	170	413	1.5382	59.949	0.001	20	20
024	3.0324	29.434	0.003	500	530	326	1.5137	61.181	0.001	20	20
107	2.9197	30.607	0.01	10	10	3 1 10	1.4911	62.205	0.02	110	120
205	2.8086	31.841	0.004	100	90	2 3 7	1.4704	63.185	0.002	20	30
008	2.7932	32.032	0.016	140	140	049	1.4601	63.688	0.01	60	60
116	2.7775	32.21	0.007	710	730	146	1.4512	64.117	0.002	130	140
210	2.7294	32.783	−0.01	20	20	1 3 11	1.4262	65.395	0.01	60	70
211	2.7093	33.034	−0.003	50	60	1 1 15	1.4028	66.642	0.03	60	50
018	2.6051	34.412	0.014	10	10	330	1.3897	67.315	0.01	70	70
214	2.4523	36.615	0.001	180	190	0 2 15	1.3771	68.054	0.02	30	40
300	2.4071	37.324	0.003	340	350	0 4 11	1.3494	69.629	0.015	20	20
301	2.3932	37.548	−0.003	90	90	2 3 10	1.3308	70.744	0.01	50	60
215	2.3293	38.625	0.006	20	20	2 2 13	1.3262	71.039	0.02	40	40
118	2.3206	38.786	0.012	20	30	2 1 15	1.3076	72.214	0.03	50	50
303	2.2905	39.303	−0.001	30	30	2 2 14	1.2673	74.889	0.012	50	50
119	2.1332	42.35	0.012	50	50	155	1.2456	76.398	0.002	30	30
305	2.1193	42.63	0.004	20	20	248	1.2262	77.839	0.004	10	10
220	2.0846	43.368	−0.002	80	90	600	1.2035	79.579	0.001	30	40
209	2.0458	44.251	0.015	10	10	4 2 10	1.1647	82.819	0.01	10	10
306	2.0216	44.799	0.002	60	70	520	1.1563	83.534	0.011	10	10
312	1.9714	45.997	−0.002	30	30	5 1 10	1.1217	86.747	0.009	10	20
224	1.953	46.457	0.001	50	50	01 20	1.1041	88.456	0.008	40	40
128	1.9521	46.49	−0.01	70	60	1 5 11	1.0932	89.611	0.003	10	10
20 10	1.9001	47.848	0.02	70	70						
314	1.8853	48.23	0.001	110	120						

phases is shown in Figure 6. Mg–O distances in [$Mg_{0.50}$] [i.e., 6 × 2.271(5) Å for Mg(1*b*)–O(10); 3 × 2.240(6) Å for Mg (2*d*′)–O(11) and 3 × 2.232(5) Å for Mg(2*d*′)–O(12)] and Ni–O distances in [$Ni_{0.50}$] [i.e., 6 × 2.272(6) Å for Ni(1*b*)–O (10); 3 × 2.234(5) Å for Ni(2d′)–O(11) and 3 × 2.227(5) Å for Ni(2*d*′)–O(12)] are relatively consistent with the sum values of the corresponding crystal radii, which are of 2.26 Å for Mg–O and 2.23 Å for Ni–O. In contrast, analysis of distance values between the centre of each 1a and 2d sites and oxygen atoms surrounding them, confirms the fact that these two sites are normally assumed to be empty. In fact, for [$Mg_{0.50}$], values of these distances are: 6 × □(1a)-O(7) = 2.524(5), 3 × □(2d)–O(8) = 2.444(6) and 3 × □(2d)-O(9) = 2.461(5) Å. The corresponding distances values for [$Ni_{0.50}$] are : 6 × □(1a)-O(7) = 2.513(5) Å, 3 × □(2d)-O(8) = 2.879(6) and 3 × □(2d)-O(9) = 2.880(5) Å. *X*–O [*X* = Sb(Fe)] and P–O distances values for both materials are grouped in Tables IV and V, respectively. Sb(Fe)–O distances-types are relatively consistent with the crystal radii values in six coordination of Sb^{5+} and Fe^{3+} ions (Shannon, 1976). P–O distances values match well with those typically observed in NASICON-type phosphates. In order to have more structural information, the bond valence sum (BVS) based on bond strength analysis (Brown and Altermatt, 1985) was also computed. As shown in Tables IV and V, the BVS values calculated for, Fe, Sb, and P sites are relatively consistent with the expected formal oxidation state of Fe^{3+}, Sb^{5+}, and P^{5+} ions. XRPD data, obtained from the "observed intensities" of the Rietveld refinement (Cu$K\alpha$1: 1.540 56 Å), of [$Mg_{0.50}$] and [$Ni_{0.50}$] phases are given in Tables VI and VII, respectively.

It is well known that in the $R\overline{3}$ space group there is an ordered distribution, along the *c*-axis, between the occupied M1(3b) sites and the empty □*M*1(3a) ones [i.e., *M*(3*b*)-□(*M* (3a)-*M*(3*b*)]. Similar cationic distribution of M cations in both [$M_{0.50}$] phases (*M* = Ni, Mg) between the vacancies □*M*(1*a*) sites and the occupied M(1b) one [i.e., M(1*b*)-□(M (1*a*)-M(1*b*)] is obtained during the structural refinements in the $P\overline{3}$ space group (Figure 7). In fact, in addition to this last-ordered cationic distribution, results of refinement show also a second-ordered distribution along the *c*-axis between *M* cations in the fully occupied *M*(2*d*′) sites and the vacancies □*M*(2*d*) ones [i.e., *M*(2*d*′)-□(*M*(2*d*)–*M*(2*d*′)] (Figure 7). Note that one can switch from the network formed by the *M*(1*a*) and *M*(1*b*) sites to the other, which is formed by the *M*(2*d*) and *M* (2*d*′) sites by a translation vector of (1/3, 2/3, ∼1/6). Taking into account the above remarks, we can admit that the

https://doi.org/10.1017/S0885715617000331 Published online by Cambridge University Press

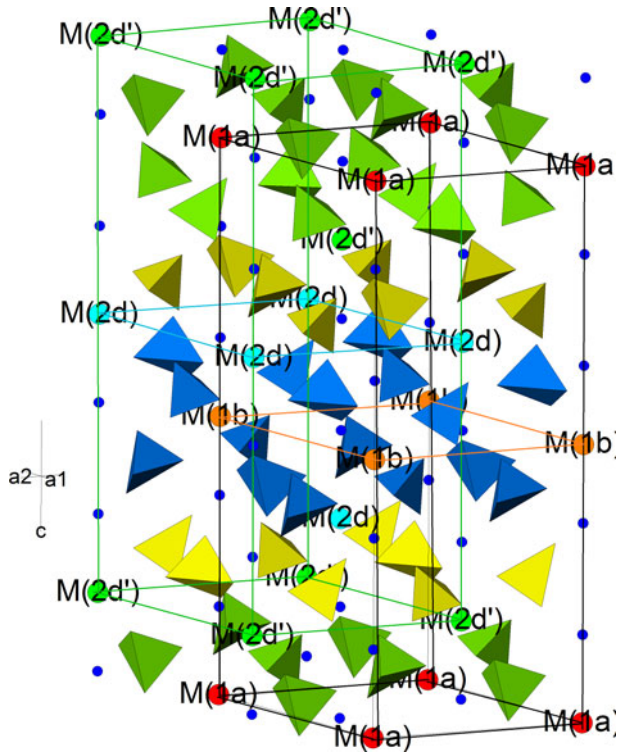

Figure 7. (Color online) Structure of $M_{0.50}SbFe(PO_4)_3$ (M = Mg, Ni) phases showing the ordered cationic distribution along the c-axis, between M cations and vacancies, of the four possible $\square M(1a)$, $M(1b)$, $\square M(2d)$, and $M(2d')$ positions of the $M1$ sites. Sb(Fe) atoms are blue circles (•), $P(1)O_4$ are yellow, $P(2)O_4$ are blue, and the $P(3)O_4$ are green.

presence of a double-ordered cationic distribution between the M cations and vacancies, within the four possible $\square M(1a)$, $M(1b)$, $\square M(2d)$ and $M(2d')$ positions of $M1$ sites, should be considered as the driving force for the unusual distortion observed when the space group switch from the $R\bar{3}$ space group to the $P\bar{3}$ one.

B. Raman spectroscopic study

In order to obtain further structural information about the nature of bonding in [$Mg_{0.50}$] and [$Ni_{0.50}$] materials, in this part of the paper, a Raman spectroscopic study was undertaken. The Raman spectrum of $Ca_{0.50}SbFe(PO_4)_3$, abbreviated as [$Ca_{0.50}$], is given here for comparison. Given that the NASICON structure contains both isolated PO_4 groups and isolated $Sb(Fe)O_6$ groups, the vibrational pattern is obviously typical of an orthophosphate. The vibrational modes of tetrahedral PO_4 molecules are well known (Nakamoto, 1986) and generally the IR and Raman spectroscopic study of orthophosphate shows that phosphate group vibrations are strong compared with the lattice modes and metal-oxygen vibrations. The two [$Mg_{0.50}$] and [$Ni_{0.50}$] Raman spectra are similar but both are slightly different from that of the [$Ca_{0.50}$] Raman spectrum (Figure 8). The relatively broadening Raman bands observed in [$Mg_{0.50}$] and [$Ni_{0.50}$] spectra [Figures 8(a) and 8(b)], in comparison with that found in the [$Ca_{0.5}$] Raman one [Figure 8(c)], may be easily related to the difference between the cationic distribution within both NASICON framework-types. In fact, both Ca^{2+} ions in $M1$ sites and $Sb^{5+}(Fe^{3+})$ within the $Ca_{0.5}SbFe(PO_4)_3$ NASICON framework are relatively orderly distributed (Aatiq *et al.*, 2006). Consequently, in this last material, every PO_4 group is surrounded by two FeO_6 octahedra and two SbO_6 octahedra. In the case of [$Mg_{0.50}$] and [$Ni_{0.50}$], the large $Sb^{5+}(Fe^{3+})$ cationic distribution within every X site of the $M_{0.50}X_2(PO_4)_3$ (M = Mg, Ni) NASICON frameworks (Tables II and III) leads to several combinations for the PO_4 group environments. So, within [$Mg_{0.50}$] and [$Ni_{0.50}$] structures, the PO_4 groups are more disturbed and consequently in addition to the broadening of the Raman bands, a shift of the modes to higher or lower wavenumbers are normally expected. In fact, the same phenomenon has already been observed in others Raman spectroscopic study of NASICON-phases (Pikl *et al.*, 1998; Junaid *et al.*, 2008; Aatiq *et al.*, 2012). The Raman band positions of the four (ν_1, ν_2, ν_3, and ν_4) PO_4 modes observed in spectra are close to those expected for NASICON-type phosphates. Their assignments were made based on data from the literature concerning some crystalline compounds (Figure 8). Thus, the symmetric non degenerate PO stretching modes (ν_1) are observed in the range 900–1020 cm^{-1}, while antisymmetric doubly degenerate PO stretching modes (ν_2) are located in the 380–480 cm^{-1} range. The symmetric, triply degenerate OPO bending (ν_3) is observed between 1050 and 1300 cm^{-1} and the triply degenerate, antisymmetric and harmonic OPO bending (ν_4) is observed in the range 530–680 cm^{-1}.

During our spectroscopic investigations, our curiosity led us to consider and compare the number of observed PO_4 Raman modes for [$Ca_{0.50}$] [$R\bar{3}$ space group] and [$Mg_{0.50}$] and/or [$Ni_{0.50}$] [$P\bar{3}$ space group]. For this reason, we have carried out the factor group analysis, which predicts the theoretically number of Raman and Infrared active modes. Given that a detailed assignment of the external modes is difficult, our discussions were focused only to the PO stretching and OPO bending modes of PO_4 ions. In fact, for [$Ca_{0.50}$] we can expect eight Raman-active stretching vibrations of PO_4 unit [$2\ \nu_1 + 6\ \nu_3$] and 10 Raman-active modes for the bending vibrations [$4\ \nu_2 + 6\ \nu_4$]. In the [$Ca_{0.50}$] Raman spectrum, the bands are reasonably well resolved and their number is approximately six for the PO stretching vibrations and six for the OPO bending ones. In compounds with $P\bar{3}$ space group, where the atoms of phosphorous occupy three crystallographic positions [i.e., $3 \times (6\ g)$], the number of expected Raman-active stretching vibrations is 24 [$6\ \nu_1 + 18\ \nu_3$] whereas for the Raman bending vibrations the expected one is 30 [$12\ \nu_2 + 18\ \nu_4$]. The number of observed bands in each Raman spectra of [$Mg_{0.50}$] and [$Ni_{0.50}$] is 10 for the stretching modes and 8 for the bending modes. It should be noticed that for compounds with $R\bar{3}$ space group, the factor group analysis predicts a maximum of eight Raman PO stretching modes. This remark clearly shows that the number of PO stretching modes observed in the Raman spectra of [$Mg_{0.50}$] and [$Ni_{0.50}$] is consistent with the crystallographic results we have obtained [i.e., $P\bar{3}$ space group].

Stretching vibrations of Sb–O are probably coupled with the P–O–P bending ν_4 mode. The frequencies found between 590 and 650 cm^{-1} in Raman spectra can be assigned empirically to Sb–O stretching modes involving Sb–O–P linkage. The same Sb–O vibrations are already observed at 597 and 652 cm^{-1} for $SbOPO_4$ in the same range of frequency and at 580 and 639 cm^{-1} for $Mn_{0.5}MSb(PO_4)_3$ (M = Al, Fe and Cr) phases (Sudarsan *et al.*, 2002; Anantharamulu *et al.*, 2009). In the lattice modes region, the translational modes of M^{2+}, Fe^{3+}, Sb^{5+}, and PO_4^{3-} ions as well as librational modes

https://doi.org/10.1017/S0885715617000331 Published online by Cambridge University Press

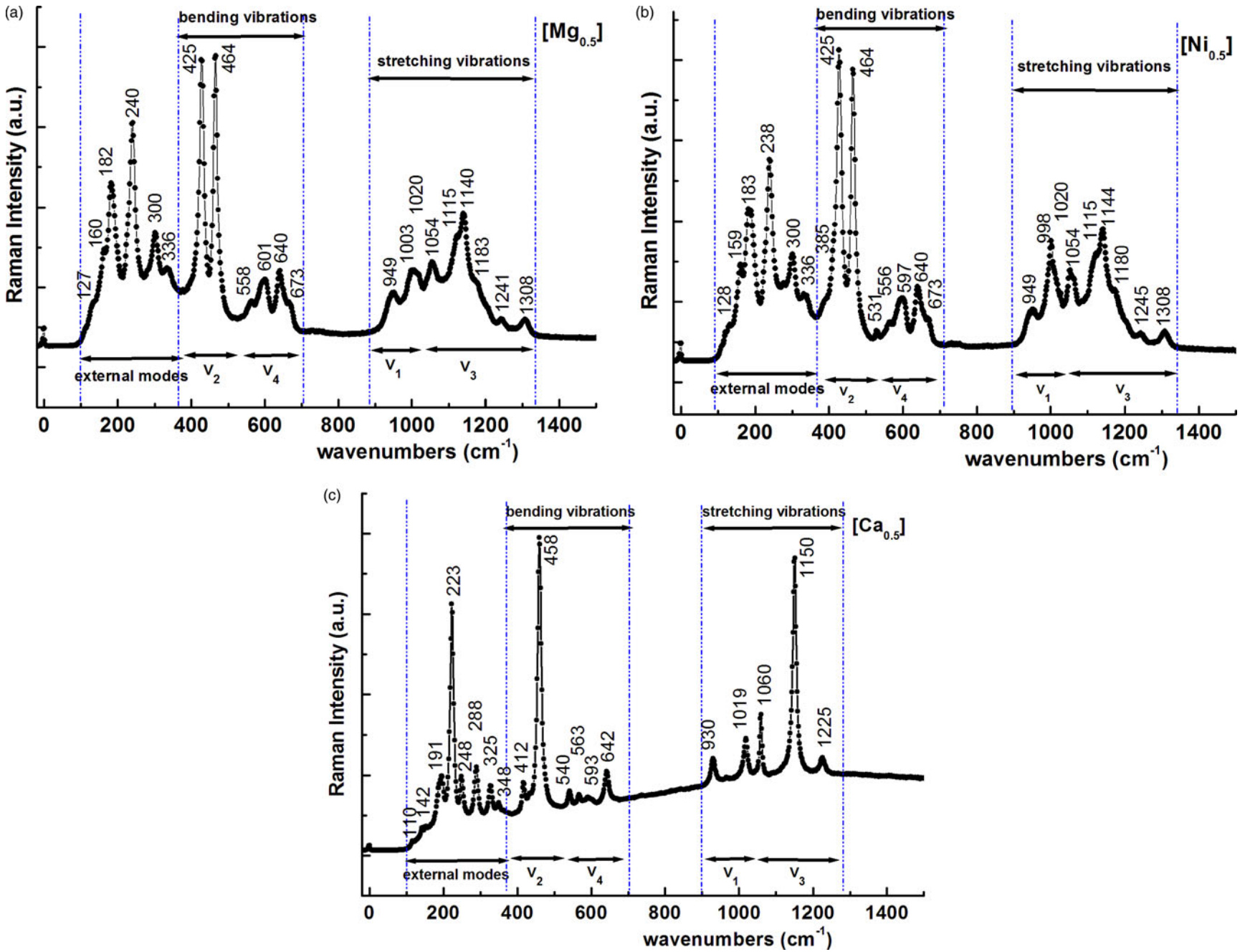

Figure 8. (Color online) Raman spectra for (a) $Mg_{0.50}SbFe(PO_4)_3$, (b) $Ni_{0.50}SbFe(PO_4)_3$, and (c) $Ca_{0.50}SbFe(PO_4)_3$ phases.

of PO_4^{3-} ions and FeO_6, SbO_6 groups should be expected. At wavenumbers below 450 cm^{-1} strong coupling between the different bending vibrations O–P–O, O–Sb–O, Sb–O–P, Sb–O–Sb is expected (Husson *et al.*, 1988). The Raman bands observed around 300 and 340 cm^{-1} could be assigned to Fe^{3+}–O stretching modes of vibrations in good agreement with the band positions observed in the range 300–370 cm^{-1} for $Li_3Fe_2(PO_4)_3$ (Butt *et al.*, 2004). The low-frequency modes observed below 270 cm^{-1} can be easily attributed to translational modes of the M^{2+}, Sb^{5+}, and $(PO_4)^{3-}$ ions.

IV. CONCLUSION

$M_{0.50}SbFe(PO_4)_3$ (M = Mg, Ni) phosphates are prepared and characterised by XRD and Raman spectroscopy. Both samples crystallise in $P\overline{3}$, which is a relatively new space group in the NASICON-type materials. In both phases, the $[SbFe(PO_4)_3]^-$ NASICON framework is preserved and a partially-ordered distribution of Sb^{5+} and Fe^{3+} ions is observed. The three M^{2+} cations of the unit cell are preferentially located as follows: one in the $M(1b)$ (0, 0, 0.5) site and the two others one are in the $M(2d')$ (1/3, 2/3, ~0.17) site. Both $M(1b)$ and $M(2d')$ sites correspond to the $M1(3b)$ sites frequently reported in NASICON structure with $R\overline{3}$ space group. Analysis of distance values between the centre of each $1a$ and $2d$ sites, which both correspond to the $M1(3a)$ sites of $R\overline{3}$ space group, and oxygen atoms surrounding them, confirms the fact that these two sites are normally assumed to be empty in $[Mg_{0.50}]$ and $[Ni_{0.50}]$ phases. Crystallographic results we obtained for both latter samples clearly show that structures of $M_{0.50}Ti_2(PO_4)_3$ (M = Mg, Co) phosphates could be solved without problems in the $P\overline{3}$ space group instead of the two $R\overline{3}c$ or $R\overline{3}$ ones. Raman study is consistent with the obtained crystal structures. In fact, results from the factor group analysis have allowed us to follow the reduction of symmetry from $R\overline{3}$ in $[Ca_{0.5}]$ to $P\overline{3}$ space group in both $[Mg_{0.50}]$ and $[Ni_{0.50}]$ phosphates. All Raman spectra show characteristic PO_4 vibrations and the stretching modes of SbO_6 groups are observed at significantly higher frequency (570 and 670 cm^{-1}) than stretching modes of FeO_6 groups (~375 cm^{-1}).

SUPPLEMENTARY MATERIAL

The supplementary material for this article can be found at https://doi.org/10.1017/S0885715617000331.

ACKNOWLEDGEMENTS

Financial support of the Moroccan Ministry of Higher Education, Scientific Research and Training of managerial staff (MESRSFC), National Center for Scientific and Technical Research (CNRST) are gratefully acknowledged. Authors are also grateful to Engineer in "SCA de l'Unités d'Appui Technique à la Recherche Scientifique (UATRS) "CNRS- Rabat, Morocco" for technical assistance; and for SCA of CNRS-Rabat for making to the disposal of our Laboratory a Panalytical X′Pert-PRO diffractometer.

Aatiq, A., Ménétrier, M., El Jazouli, A., and Delmas, C. (**2002**). "Structural and lithium intercalation studies of $Mn_{(0.5-x)}Ca_xTi_2(PO_4)_3$ phases ($0 \leq x \leq 0.50$)," Solid State Ion. **150**, 391–405.

Aatiq, A., Hassine, R., Tigha, R., and Saadoune, I. (**2005**). "Structures of two newly synthesized $A_{0.50}SbFe(PO_4)_3$ (A = Mn, Cd) NASICON phases," Powder Diffr. **20**, 33–39.

Aatiq, A., Tigha, R., Hassine, R., and Saadoune, I. (**2006**). "Crystallochemistry and structural studies of two newly $CaSb_{0.50}Fe_{1.50}(PO_4)_3$ and $Ca_{0.50}SbFe(PO_4)_3$ NASICON phases," Powder Diffr. **21**, 45–51.

Aatiq, A., Tigha, R., and Benmokhtar, S. (**2012**). "Structure, infrared and Raman spectroscopic studies of new $Sr_{0.50}SbFe(PO_4)_3$ and $SrSb_{0.50}Fe_{1.50}(PO_4)_3$ NASICON phases," J. Mater. Sci. **47**, 1354–1364.

Aatiq, A., Tigha, R., Fakhreddine, R., and Marchoud, A. (**2015**). "Structure and spectroscopic characterization of the two $PbSb_{0.5}Fe_{1.5}(PO_4)_3$ and $Pb_{0.5}SbFe(PO_4)_3$ phosphates with NASICON type-structure," J. Mater. Environ. Sci. **6**(12), 3483–3490.

Alami Talbi, M., Brochu, R.; Parent, C., Rabardel, L., and Le Flem, G. (**1994**). "The new phosphates $Ln_{1/3}Zr_2(PO_4)_3$ (Ln = Rare Earth)," J. Solid State Chem. **110**, 350–355.

Anantharamulu, N., Rao, K. K., Vithal, M., and Prasad, G. (**2009**). "Preparation, characterization, impedance and thermal expansion studies of $Mn_{0.5}MSb(PO_4)_3$ (M = Al, Fe and Cr)," J. Alloys Compd. **479**, 684–691.

Anuar, N. K., Adnan, S. B. R. S., and Mohamed, N. S. (**2014**). "Characterization of $Mg_{0.5}Zr_2(PO_4)_3$ for potential use as electrolyte in solid state magnesium batteries," Ceram. Int. **40**, 13719–13727.

Barré, M., Crosnier-Lopez, M. P., Le Berre, F., Emery, J., Suard, E., and Fourquet, J. L. (**2005**). "Room temperature crystal structure of $La_{1/3}Zr_2(PO_4)_3$, a NASICON-type compound," Chem. Mater. **17**, 6605–6610.

Barré, M., Le Berre, F., Crosnier-Lopez, M. P., Bohnke´, O., Emery, J., and Fourquet, J. L. (**2006**). "La^{3+} Diffusion in the NASICON-type compound $La_{1/3}Zr_2(PO_4)_3$: X-ray thermodiffraction, ^{31}P NMR, and ionic conductivity investigations," Chem. Mater. **18**, 5486–5491.

Barré, M., Crosnier-Lopez, M. P., Le Berre, F., Suard, E., and Fourquet, J. L. (**2007**). "Synthesis and structural study of a new NASICON-type solid solution: $Li_{1-x}La_{x/3}Zr_2(PO_4)_3$," J. Solid State Chem. **180**, 1011–1019.

Barth, S., Olazcuaga, R., Gravereau, P., le Flem, G., and Hagenmüller, P. (**1993**). "$Mg_{0.5}Ti_2$ $(PO_4)_3$: a new member of the NASICON family with low thermal expansion," Mater. Lett. **16**, 96–101.

Benmokhtar, S., El Jazouli, A., Aatiq, A., Chaminade, J. P., Gravereau, P., Wattiaux, A., Fournes, L., and Grenier, J. C. (**2007**). "Synthesis, structure and characterisation of $Fe_{0.50}Ti_2(PO_4)_3$: a new material with NASICON-like structure," J. Solid State Chem. **180**, 2004–2012.

Brown, I. D. and Altermatt, D. (**1985**). "Bond-valence parameters obtained from a systematic analysis of the inorganic crystal structure database," Acta Crystallogr. B: Struct. Sci. **B41**, 244–247.

Bykov, D. M., Gobechia, E. R., Kabalov, Yu. K., Orlova, A. I., and Tomilin, S. V. (**2006**). "Crystal structures of lanthanide and zirconium phosphates with general formula $Ln_{0.33}Zr_2(PO_4)_3$, where Ln = Ce, Eu, Yb)," J. Solid State Chem. **179**, 3101–3106.

Butt, G., Sammes, N., Tompsett, G., Smirnova, A., and Yamamoto, O. (**2004**). "Raman spectroscopy of superionic Ti-doped $Li_3Fe_2(PO_4)_3$ and $LiNiPO_4$ structures," J. Power Sources **134**, 72–79.

Crosnier-Lopez, M. P., Barré, M., Le Berre, F., and Fourquet, J. L. (**2006**). "Electron-irradiation induced phase transformation in $La_{1/3}Zr_2(PO_4)_3$: La^{3+} displacement in a preserved NASICON framework," J. Solid State Chem. **179**, 2714–2720.

Delmas, C., Viala, J. C., Olazcuaga, R., Le Flem, G., Hagenmuller, P., Cherkaoui, F., and Brochu, R. (**1981**). "Ionic conductivity in Nasicon-type phases $Na_{1+x}Zr_{2-x}Lx(PO_4)_3$ (L = Cr, In, Yb)," Solid State Ion. **3/4**, 209–214.

Derouet, J., Beaury, L., Porcher, P., Olazcuaga, R., Dance, J. M., Le Flem, G., El Bouari, A., and El Jazouli, A. (**1999**). "A new NASICON-type phosphate: $Co_{0.5}Ti_2(PO_4)_3$ II. Simulation of optical and magnetic properties," J. Solid State Chem. **143**, 230–238.

El Bouari, A., El Jazouli, A., Dance, J. M., Le Flem, G., Olazcuaga, R. (**1994**). "A New NASICON-Like Phosphate $Co_{0,5}Ti_2(PO_4)_3$", Adv. Mater. Res. **1–2**, 173–176.

Hans, W. and Ulrich, M. (Eds.) (**2004**). *International Tables for Crystallography Vol. A1: Symmetry Relation between Space Group* (Kluwer Academic Publishers, Dordrecht/Boston/London), 1th ed., p. 286; 310.

Husson, E., Genet, F., Lachgar, A., and Piffard, Y. (**1988**). "The vibrational spectra of some antimony phosphates," J. Solid State Chem. **75**, 305–312.

Junaid Bushiri, M., Antony, C. J., and Aatiq, A. (**2008**). "Raman and FTIR studies of the structural aspects of NASICON-type crystals; AFeTi $(PO_4)_3$ (A = Ca, Cd)," J. Phys. Chem. Solids **69**, 1985–1989.

Le Bail, A., Duroy, H., and Fourquet, J. L. (**1988**). "Ab-initio structure determination of $LiSbWO_6$ by X-ray powder diffraction," Mater. Res. Bull. **23**, 447–452.

Nakamoto, K. (**1986**). *Infrared and Raman Spectra of Inorganic and Coordination Compounds* (Wiley–Interscience, New York), 4th ed., p. 138.

Olazcuaga, R., Dance, J. M., Le Flem, G., Derouet, J., Beaury, L., Porcher, P., El Bouari, A., and El Jazouli, A. (**1999**). "A new NASICON-type phosphate $Co_{0.5}Ti_2(PO_4)_3$: I. Elaboration, optical and magnetic properties," J. Solid State Chem. **143**, 224–229.

Padhi, A. K., Nanjundaswamy, K. S., Masquelier, C., and Goodenoogh, J. B. (**1997**). "Mapping of transition metal redox energies in phosphates with NASICON structure by lithium intercalation," J. Electrochem. Soc. **144** (8), 2581–2586.

Pikl, R., de Waal, D., Aatiq, A., and El Jazouli, A. (**1998**). "Vibrational spectra and factor group analysis of $Mn_{(0.5+x)}Ti_{(2-2x)}Cr_{2x}(PO_4)_3$ $\{0 \leq x \leq 0.50\}$," Vibr. Spectrosc. **16**, 137–143.

Rodriguez-Carvajal, J. (**1997**). *Fullprof, Program for Rietveld refinement* (Laboratoire Léon Brillouin (CEA-CNRS), Saclay, France).

Roy, R., Vance, E. R., and Alamo, J. (**1982**). " [NZP], A new radiophase for ceramic nuclear waste forms," Mat. Res. Bull. **17**, 585–589.

Shannon, R. D. (**1976**). "Revised effective ionic and systematic studies of interatomic distances in halides and chalcogenides," Acta Crystallogr. A: Cryst. Phys. Diffr. Theor. Gen. Crystallogr. **32**, 751–767.

Sudarsan, V., Muthe, K. P., Vyas, J. C., and Kulshreshtha, S. K. (**2002**). "PO_4^{3-} tetrahedra in $SbPO_4$ and $SbOPO_4$: a ^{31}P NMR and XPS study," J. Alloys Compd. **336**, 119–123.

Woodcock, D. A., Lightfoot, P., and Smith, R. I. (**1999**). "Powder neutron studies of three low thermal expansion in the NZP family: $K_{0.5}Nb_{0.5}Ti_{1.5}(PO_4)_3$, $BaTi_2(PO_4)_3$ and $Ca_{0.25}Sr_{0.25}Zr_2(PO_4)_3$," J. Mater. Chem. **9**, 2631–2636.

Zhao, Y., Wei, Z., Pang, Q., Wei, Y., Cai, Y., Fu, Q., Du, F., Sarapulova, A., Ehrenberg, H., Liu, B., and Chen, G. (**2017**). "NASICON-type $Mg_{0.5}Ti_2(PO_4)_3$ negative electrode material exhibits different electrochemical energy storage mechanisms in na-ion and li-ion batteries," ACS Appl. Mater. Interfaces **9**(5), 4709–4718.

https://doi.org/10.1017/S0885715617000331 Published online by Cambridge University Press